SUPPLEMENTARY INFORMATION

Tryptophan-accelerated electron flow across a protein-protein interface

Kana Takematsu,[a,†] Heather Williamson,[a,†] Ana María Blanco-Rodríguez,[b] Lucie Sokolová,[c] Pavle Nikolovski,[a] Jens T. Kaiser,[a] Michael Towrie,[d] Ian P. Clark,[d] Antonín Vlček, Jr.,*[,b,e] Jay R. Winkler,*[,a] and Harry B. Gray*[a]

[a] Beckman Institute, California Institute of Technology, Pasadena, CA 91125, USA
[b] Queen Mary University of London, School of Biological and Chemical Sciences, Mile End Road, London E1 4NS, United Kingdom
[c] Institute of Physical and Theoretical Chemistry, Goethe-Universität, Max-von-Laue-Str. 7, 60438 Frankfurt am Main, Germany
[d] Central Laser Facility, Research Complex at Harwell, Science and Technology Facilities Council, Rutherford Appleton Laboratory, Harwell Oxford, Didcot, Oxfordshire, OX11 0FA, UK
[e] J. Heyrovský Institute of Physical Chemistry, Academy of Sciences of the Czech Republic, Dolejškova 3, CZ-182 23 Prague, Czech Republic
E-mail: hbgray@caltech.edu, a.vlcek@qmul.ac.uk, winklerj@caltech.edu

† These authors contributed equally to this work.

X-ray diffraction

Table S1. X-ray data collection, refinement statistics, and validation for **Re126W122Cu^{II}**.

Data collection	
Wavelength, Å	0.9795
Unit cell, Å	42.391, 93.215, 109.383
Space group	F222
Resolution range, Å	35.00-1.70 (1.79-1.70)
No. of unique reflections	12078 (1733)
Multiplicity	5.2 (5.1)
Completeness, %	99.5 (99.5)
$\langle I/\sigma(I)\rangle$	8.6 (1.8)
R_{pim}	0.047 (0.469)
Wilson B-value, Å^2	23.022
Refinement statistics	
Resolution range, Å	27.35-1.70
No. of reflections used	12064
Free R reflections, %	4.8
R/R_{free}	0.1963/0.2360
Rmsd bond length, Å	0.015
Rmsd bond angle, degree	1.77
<B>	30.5
Ramachandran analysis, %	
No. of residues in	
Favored regions	94.4
Outlier regions	1.6
PDB entry	4K9J

*Data for outermost shell given in parentheses

TRIR Spectra

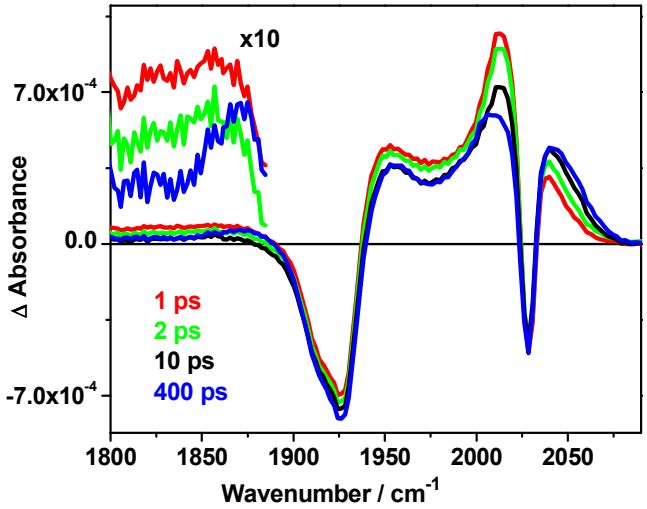

Figure S1. Picosecond TRIR spectra of ~1 mM **Re126W122Cu^{II}** in 20 mM KP_i buffer in D_2O (pD = 7.1) measured at selected time delays after ~50 fs, 400 nm laser pulse excitation. Experimental points are separated by *ca*. 2.2 cm^{-1}.

TRIR dynamic shifts and shape-fitting

Figures 1 and S1 show that the transient IR bands undergo dynamic up-shift and narrowing on pico- and nanosecond timescales, which are most apparent for the CT1 band. These shifts and shape-changes preclude kinetics analysis based on time-dependent absorbance at wavenumbers corresponding to peak-maxima. To overcome this problem, we have fitted the TRIR spectra to sums of Gaussians, determining the areas, peak wavenumbers, and widths of the CT1 and CS2 bands and of the ~1925 cm^{-1} bleach that was modeled by two Gaussians. Representative fits are shown in Figure S2. The kinetics analysis is based on time-dependent band areas, see Figure 2.

The CT1 band shift occurs with a multiexponential dynamics from the initial position of ~2042 cm^{-1} to final positions of 2051 and 2055 cm^{-1} for **Re126W122Cu^{II}** and **Re126W122Cu^{I}**, respectively, that are reached at time delays of ~200 ns. Part of the shift (3-4 cm^{-1}) occurs on the picosecond timescale, attributable to vibrational cooling.[1] In the nanosecond range, the following shift time constants (amplitudes) were determined: 8.6±2.3 ns (~2.2 cm^{-1} amplitude) and 74±8 ns (3.4±0.3 cm^{-1}) for **Re126W122Cu^{II}**; 7.1±2.3 ns (7.4±0.4 cm^{-1}) and 30±4 ns (3.2±0.5 cm^{-1}) for **Re126W122Cu^{I}** (Figure S3). Although the magnitudes of these shifts resemble those attributed to relaxation dynamics for other Re-labeled azurins,[1-3] they occur with much slower rates that are comparable to the ET kinetics. Instead of assigning this effect to a single-band shift, it is likely that most of the observed CT1 nanosecond dynamic shift arises from the overlap of two different bands with time-dependent relative intensities, namely, a rapidly decaying ~2042 cm^{-1} band of the dimer and a band at 2051-2055 cm^{-1} due to the CT state of the unreactive monomer decaying with a 220 ns (Cu^{I}) or ~700 ns (Cu^{II}) lifetime. (Simulations of two overlapping broad Gaussian functions have confirmed that this behavior gives rise to a single Gaussian-like band with a time-dependent peak position.) A slow relaxation of the protein-protein interface after excitation also could contribute to the 7-9 ns shift component.

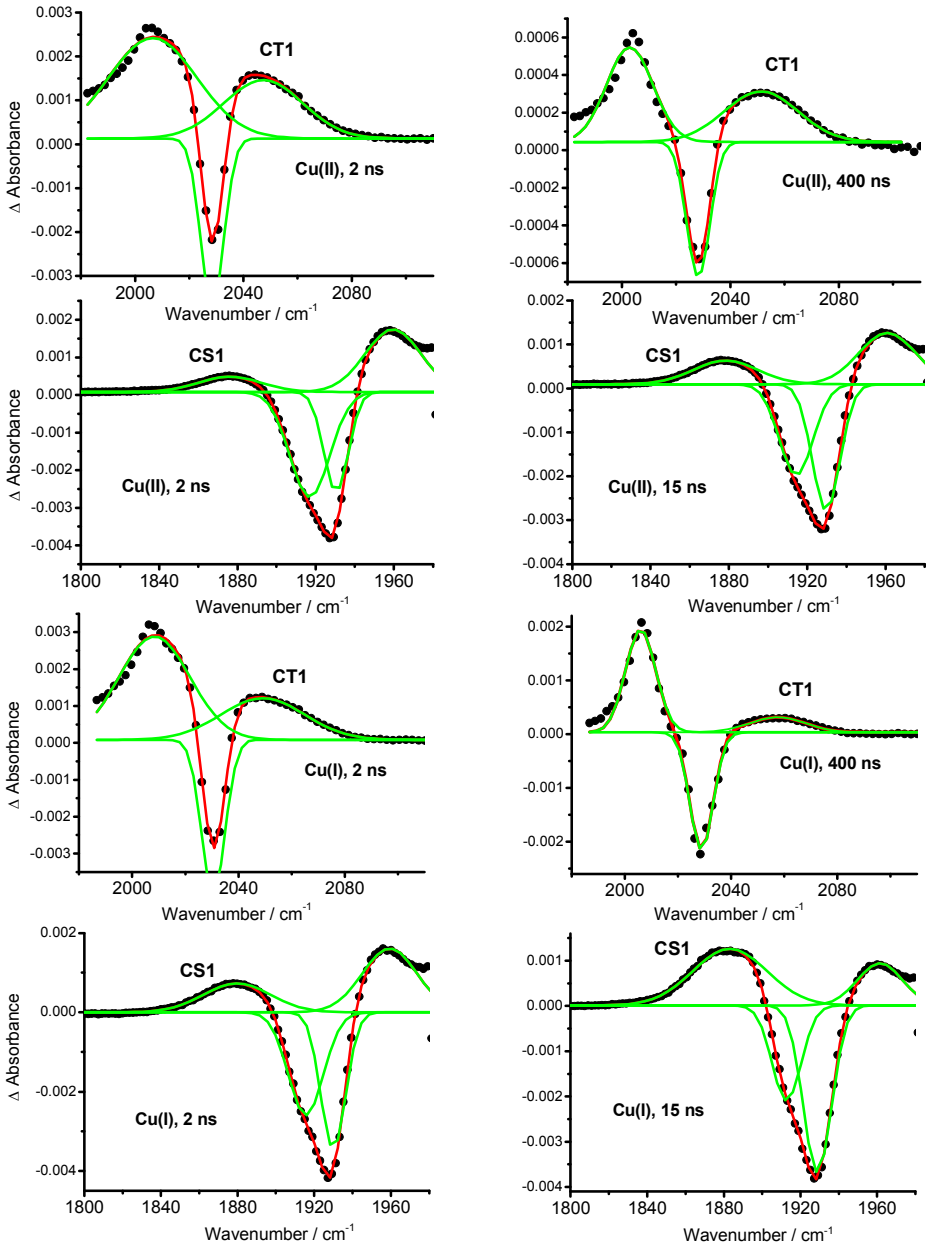

Figure S2. Examples of shape-fitting of TRIR spectra to determine parameters of the CT1, CS2, and combined ~1925 cm^{-1} bleach. Experimental conditions as for Figure 1.

The shapes and positions of the picosecond and early nanosecond CT1 bands of **Re126W122Cu^{II,I}** resemble those observed in TRIR spectra of **Re124X122Cu^{II,I}** (X = aromatic amino acid W, Y, or F), suggesting similar excited-state character involving interactions between dmp and the aromatic side-chains and/or restricted structural relaxation.[1,2] On the other hand, the 23-28 cm^{-1} difference between the CT1 band position at time delays >200 ns and the

corresponding 2028 cm^{-1} ground-state bleach is comparable to those observed[1,3] for $Re(CO)_3(dmp)(H107)AzCu^{II}$ and $Re(CO)_3(dmp)(H124)(K122)AzCu^{II}$, in accord with an unperturbed Re→dmp ^{3}MLCT character of the monomer excited state, where the W122(indole) and dmp are far apart.

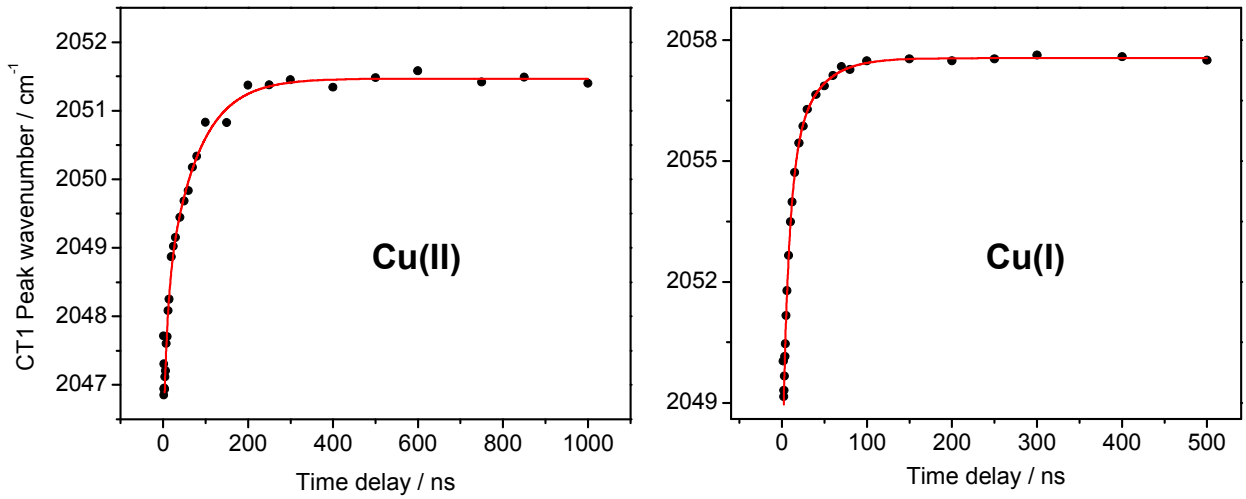

Figure S3. Time-dependent peak-energy of the CS1 band measured by ns TRIR spectroscopy. Experimental conditions as for Figure 1.

The CS2 band of **Re126W122Cu^{II}** initially appears as a broad band at about 1876 cm^{-1} (Cu^{II}) or ~1879 cm^{-1} (Cu^{I}). It broadens and upshifts to 1885-1889 cm^{-1} on 100-ns and 1 μs (Cu^{II}); 10-ns and μs (Cu^{I}) timescales, apparently due to a shoulder developing on its high-energy side. These CS2 band changes are attributable to changing the environment around $Re(CO)_3(dmp^{\bullet-})$ by, e.g. $W122^{\bullet+}$ deprotonation and, for Cu^{I}, $W122^{\bullet+}$ reduction and RP_α/RP_β equilibration, see the main text.

Kinetics analysis

To simplify the kinetics model, we omitted the subnanosecond dynamics and began our analysis with the relaxed ^{3}CT state, whose formation is assumed to be much faster than any subsequent reaction. The kinetics scheme is shown in Figure S1.

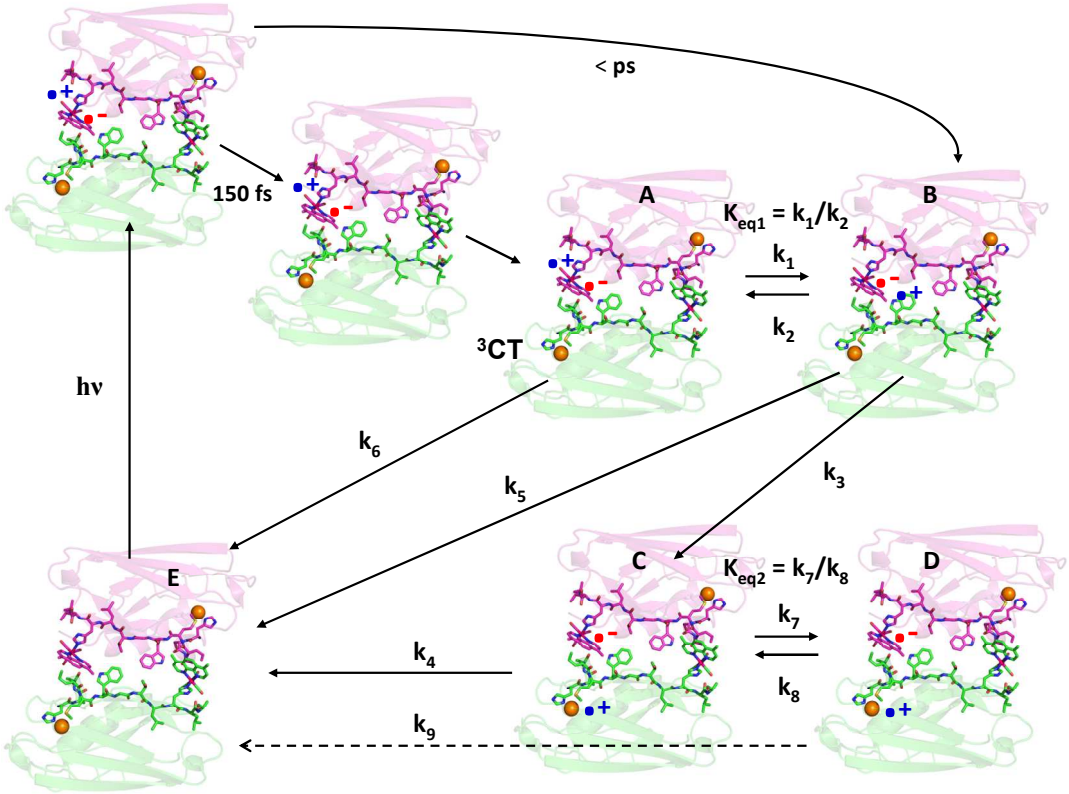

Scheme S1. Kinetics model of the **Re126W122Cu^I** photocycle.
(Single-step intermolecular *Re//←Cu^I ET is not included in the mechanism since the similarity of the Cu^{II} and Cu^I kinetics points to a common nature of the initial charge separation step, that is W122→//*Re. Both the intramolecular single-step *Re←Cu^I and sequential *Re←W122←Cu^I ET are assumed to be uncompetitive with k_1 and k_3.)

A system of linear differential equations (S1) was evaluated numerically using a Matlab code written at Caltech.

$$\frac{d[A]}{dt} = -(k_1 + k_6)[A] + k_2[B] \qquad \text{(S1a)}$$

$$\frac{d[B]}{dt} = k_1[A] - (k_2 + k_3 + k_5)[B] \qquad \text{(S1b)}$$

$$\frac{d[C]}{dt} = k_3[B] - (k_4 + k_7)[C] + k_8[D] \quad \text{(S1c)}$$

$$\frac{d[D]}{dt} = k_7[C] - k_8[D] \quad \text{(S1d)}$$

$$\frac{d[E]}{dt} = k_6[A] + k_5[B] + k_4[C] \quad \text{(S1e)}$$

1) Zero initial conditions were assumed for all photoproduced intermediates:
$[A]_0 = 1$, $[B]_0 = [C]_0 = [D]_0 = [E]_0 = 0$

2) Reversibility between the CT and CS states[2,4] and between the two forms of the redox product was assumed:

$$k_2 = k_1/K_{eq1} \quad \text{(S2a)}$$

$$k_8 = k_7/K_{eq2} \quad \text{(S2b)}$$

3) For Cu^{I}, k_3 was fixed at $(30\ ns)^{-1}$ based on **Re124W122Cu^{I}** kinetics (Scheme 1). For Cu^{II}, $k_3 = 0$.

4) For Cu^{I}, k_6 was fixed at $(670\ ns)^{-1}$ based on excited state decay of the **Re126W122Cu^{I}** monomer.

For Cu^{II}, k_6 was fixed at $(220\ ns)^{-1}$ based on excited state decay of the **Re126W122Cu^{II}** monomer.

5) Population A can be decoupled from the rest of the model. The analytical expression for $[A]$ is:

$$[A] = a_1 e^{-\lambda_1 t} + a_2 e^{-\lambda_2 t} \quad \text{(S3a)}$$

with coefficients $a_1 = \frac{\alpha - \lambda_2}{\lambda_1 - \lambda_2}, \quad a_2 = \frac{\lambda_1 - \alpha}{\lambda_1 - \lambda_2}$ (S3b)

and observables $\lambda_{1,2} = -\lambda_{\pm} = -\frac{-(\alpha+\beta) \pm \sqrt{(\alpha-\beta)^2 + 4k_1k_2}}{2}$ (S3c)

where $\alpha = k_1 + k_6$ and $\beta = k_2 + k_3 + k_5$.

To simulate the observed excited state lifetimes, we varied k_1, K_{eq1} (which inherently changes k_2), and k_5 in equations S3 and obtained the following values (Scheme 2):

For Cu^{II}: $k_1 = (7\ ns)^{-1}$, $k_2 = (9\ ns)^{-1}$, $k_5 = (25\ ns)^{-1}$
For Cu^{I}: $k_1 = (7\ ns)^{-1}$, $k_2 = (8\ ns)^{-1}$, $k_5 = (70\ ns)^{-1}$

Using equations S3a-c, k_1, k_2, and k_5 can also be expressed analytically in terms of k_3, k_6, a_1, a_2, λ_1, and λ_2:

$$k_1 = \frac{1}{2}[\lambda_1(1+a_1-a_2)+\lambda_2(1-a_1+a_2)]-k_6 \quad \text{(S3d)}$$

$$k_5 = \frac{1}{k_1}[\lambda_1\lambda_2 - k_6(a_2-a_1)(\lambda_1-\lambda_2)-\alpha^2+(\alpha-k_3)k_1] \quad \text{(S3e)}$$

$$k_2 = \lambda_1+\lambda_2-k_1-k_6-k_3-k_5 \quad \text{(S3f)}$$

6) To obtain the rate constants k_4, k_7, and k_8 (where the latter two are related by K_{eq2}) we simulated the whole mechanism using eqs. S1a-e and fixing k_1, k_2, and k_5 to the above values. $k_4 \approx k_7$ was assumed as TA and TRIR data showed that the 220 ns and 6 μs BET kinetics components have comparable amplitudes.
k_4 and K_{eq2} were varied until the population decay rates of C+D were equivalent to the observed BET rates and obtained the following values (Scheme 2):

For Cu^{I}: $k_4 = (375\ ns)^{-1}$, $k_7 = (375\ ns)^{-1}$, $k_8 = (3\ \mu s)^{-1}$

7) Using the above procedure, we obtained the following values of observable lifetimes:
For Cu^{II}: excited state decays: 3.6 ns and 43 ns.
For Cu^{I}: excited state decays: 3.4 ns and 41 ns; BET: 200 ns and 6.25 μs.

The Matlab code could easily be adjusted to include an additional BET pathway from D to E or multiple redox products. Here, we only present the simplest kinetics scheme that still accounts for the experimental observables.

LILBID mass spectra

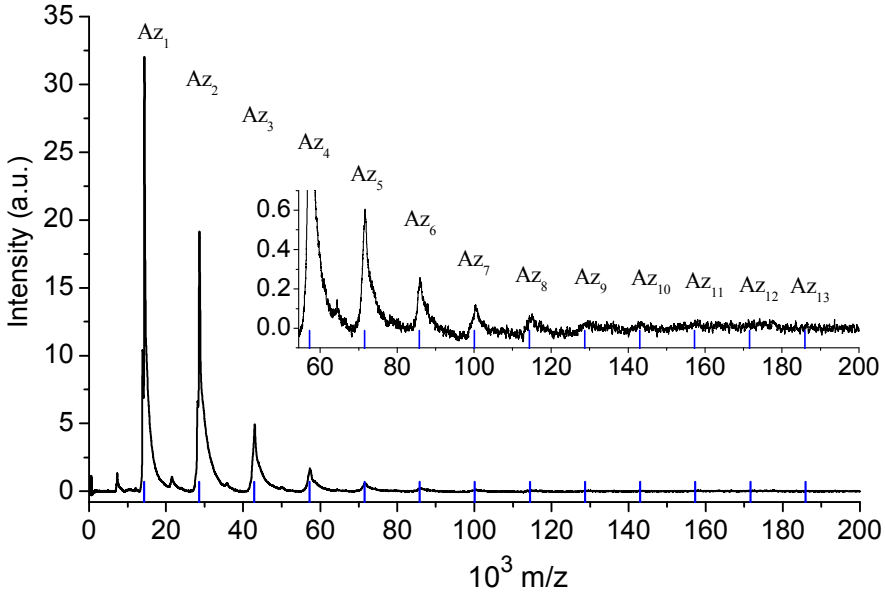

Figure S4. LILBID mass spectrum of 0.27 mM **Re126W122Cu^{II}** in 50 mM NH_4P_i (pH = 7), measured at the harsh mode.

Luminescence decay of Re126W122Cu^{II}: data analysis

Information on the solution composition was obtained by analyzing the concentration dependence of luminescence decay kinetics. First, the luminescence intensity decays were fitted globally to triexponential kinetics with linked lifetimes using equations S4a and S4b for data collected at Caltech and the JH-Institute, respectively:

$$I_{obs}(t) = a'_1 \exp(t/\tau_1) + a'_2 \exp(-t/\tau_2) + a'_3 \exp(-t/\tau_3); \quad 20\ \text{ns} \le t \le 9.8\ \mu\text{s} \qquad \text{(S4a)},$$

$$I_{obs}(t) = a'_1 \exp(t/\tau_1) + a'_2 \exp(-t/\tau_2) + a'_3; \quad 20\ \text{ns} \le t \le 880\ \text{ns} \qquad \text{(S4b)},$$

where τ_1 (~48 ns) and τ_2 (~220 ns) are attributed to the dimer and monomer emission, respectively. The relative pre-exponential factors a_1, a_2 (expressed as fraction of the total **Re126W122Cu^{II}** emission intensity at t = 0: $a_1 = \frac{a_1'}{a_1' + a_2'}$) provide information on the solution composition.

Two models were explored:

Model 1. The two protein folds in the dimer are oriented asymmetrically, such that only one Re moiety is able to oxidize tryptophan across the interface. The fast decay τ_1 is attributed to the reactive Re center, whereas τ_2 corresponds to the unreactive Re site in the dimer and the monomer. The kinetics model is as follows:

$$A + A = A\text{-}A \quad \text{(S5)},$$

where A = **Re126W122Cu^{II}**. If Y = [**Re126W122Cu^{II}**] + [**(Re126W122Cu^{II})$_2$**] and α = dimer fraction in solution, then the binding constant K is:

$$K = \frac{[\text{A-A}]}{[\text{A}]^2} = \frac{\alpha}{(1-\alpha)^2 Y} \quad \text{(S6a)}$$

$$\alpha = \frac{[\text{A-A}]}{[\text{A}]+[\text{A-A}]} = \frac{[\text{A-A}]}{Y}$$

Since the observed luminescence originates from both monomer and dimer species, we write:

$$I_{obs} = (1-\alpha)I_{\text{A}} + \alpha I_{\text{A-A}} = (1-\alpha)\exp(-t/220) + \alpha[\frac{1}{2}\exp(-t/220) + \frac{1}{2}\exp(-t/48)] =$$
$$= (1-\frac{\alpha}{2})\exp(-t/220) + \frac{\alpha}{2}\exp(-t/48) = a_1\exp(-t/48) + a_2\exp(-t/220) \quad \text{(S7)},$$

where the lifetimes τ_1, τ_2 are expressed in ns. Considering that a_1 = ½α and the spectroscopically determined concentration X (calculated from the absorbance at 632 nm) can be expressed as:

$$X = [\text{A}] + 2[\text{A-A}] = (1+\alpha)Y \quad \text{(S8)},$$

we can determine the dimerization constant K by fitting the concentration dependence of a_1 (Figure 5) according to eq. S9:

$$K = \frac{2a_1(1+2a_1)}{(1-2a_1)^2 X} \quad \text{(S9)},$$

The fit yields a K value of 4.0×10^4 M^{-1} but fails to reproduce the behavior at high concentrations, see Figure 5.

Model 2. The A-A dimer is symmetric, such that both Re sites are capable of oxidizing the interfacial tryptophans. τ_1 corresponds to the dimer and τ_2 to the monomer. K is still given by eqs. S5 and S6, while the expression for observed luminescence changes to:

$$I_{obs} = (1-\alpha)I_{A} + \alpha I_{A\text{-}A} = (1-\alpha)\exp(-t/220) + \alpha\exp(-t/48) \quad \text{(S10)}$$

In this case, $a_1 = \alpha$, which changes the expression for the binding constant K to

$$K = \frac{a_1(1+a_1)}{(1-a_1)^2 X} \quad \text{(S11)}$$

The corresponding fit (Figure 7 – red curve) reproduces the observed behavior over the whole concentration range, yielding a K value of 6.1×10^3 M^{-1}.

References

(1) Blanco-Rodríguez, A. M.; Busby, M.; Ronayne, K. L.; Towrie, M.; Sýkora, J.; Hof, M.; Záliš, S.; Grădinaru, C.; Di Bilio, A. J.; Crane, B. R.; Gray, H. B.; Vlček, J., A. *J. Am. Chem. Soc.* **2009**, *131*, 11788-11800.

(2) Blanco-Rodríguez, A. M.; Di Bilio, A. J.; Shih, C.; Museth, A. K.; Clark, I. P.; Towrie, M.; Cannizzo, A.; Sudhamsu, J.; Crane, B. R.; Sýkora, J.; Winkler, J. R.; Gray, H. B.; Záliš, S.; Vlček, A., Jr. *Chem. Eur. J.* **2011**, *17*, 5350 – 5361.

(3) Blanco-Rodríguez, A. M.; Busby, M.; Grădinaru, C.; Crane, B. R.; Di Bilio, A. J.; Matousek, P.; Towrie, M.; Leigh, B. S.; Richards, J. H.; Vlček, A., Jr.; Gray, H. B. *J. Am. Chem. Soc.* **2006**, *128*, 4365-4370.

(4) Shih, C.; Museth, A. K.; Abrahamsson, M.; Blanco-Rodriguez, A. M.; Di Bilio, A. J.; Sudhamsu, J.; Crane, B. R.; Ronayne, K. L.; Towrie, M.; Vlček, A., Jr.; Richards, J. H.; Winkler, J. R.; Gray, H. B. *Science* **2008**, *320*, 1760-1762.